Slow DNA Transport through Nanopores in Hafnium Oxide Membranes

Joseph Larkin,[†,#] Robert Henley,[†,#] David C. Bell,[‡] Tzahi Cohen-Karni,[§] Jacob K. Rosenstein,[⊥] and Meni Wanunu[†,*]

[†]Departments of Physics and Chemistry/Chemical Biology, Northeastern University, Boston, Massachusetts 02115, United States, [‡]School of Engineering and Applied Sciences, Harvard University, Cambridge, Massachusetts 02138, United States, [§]David H. Koch Institute for Integrative Cancer Research, Massachusetts Institute of Technology, Cambridge, Massachusetts 02139, United States, and [⊥]School of Engineering, Brown University, Providence, Rhode Island 02912, United States. [#]J. Larkin and R. Henley have contributed equally to this manuscript.

ABSTRACT We present a study of double- and single-stranded DNA transport through nanopores fabricated in ultrathin (2−7 nm thick) free-standing hafnium oxide (HfO_2) membranes. The high chemical stability of ultrathin HfO_2 enables long-lived experiments with <2 nm diameter pores that last several hours, in which we observe >50 000 DNA translocations with no detectable pore expansion. Mean DNA velocities are slower than velocities through comparable silicon nitride pores, providing evidence that HfO_2 nanopores have favorable physicochemical interactions with nucleic acids that can be leveraged to slow down DNA in a nanopore.

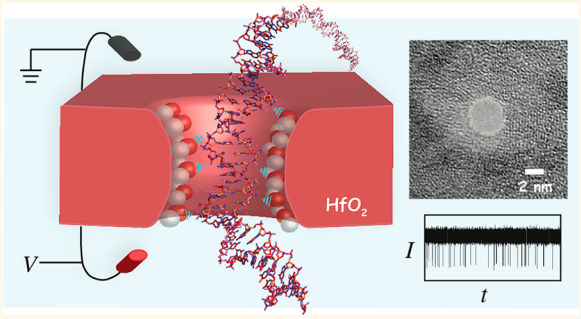

KEYWORDS: single-molecule · translocations · DNA sequencing · atomic layer deposition

Natural and synthetic nanopores are increasingly popular tools for characterizing various biomolecules and their complexes at the single-molecule level.[1−3] Pioneered by the demonstration of voltage-driven, single-file transport of DNA molecules through a lipid-embedded α-hemolysin protein channel,[4] nanopore research has been fueled by new potential applications for genomic analysis and DNA sequencing.[5−7] In this method, electrochemical bias applied across a nanopore in aqueous electrolyte medium generates highly localized electrophoretic forces that are used to drive biopolymers through the nanopore. Discrete fluctuations in the ion current as a function of time yield information about biopolymer size, sequence, and concentration. Nanopores are attractive apparatuses for mapping[8,9] and quantifying[10−14] interactions within biomolecular complexes. Fabrication of synthetic nanopores by irradiation using electron beams,[15] ion beams,[16] and He beams[17] has gained popularity due to a more flexible pore geometry that accommodates various-sized biopolymers, as well as the intriguing potential to explore various biopolymer/materials interfaces.

A significant hurdle for nanopore-based analysis of DNA, RNA, and protein molecules has been that the reported translocation speeds are too fast relative to the speed at which current is detected using conventional patch-clamp amplifiers.[2] Various systematic explorations of biomolecular transport through synthetic nanopores suggest that biopolymer detection requires a combination of nanopores with optimal geometry (diameter and thickness),[18−23] surface properties,[24−26] and improved temporal resolutions.[23,27] While nanopores in silicon oxide[28] and silicon nitride (SiN_x) membranes with various geometries have been thoroughly studied, their physical stability is compromised by unavoidable chemical damage during[29,30] and after[31] pore fabrication. This material instability has set a practical limit on membrane thicknesses that can be used for SiN_x membranes (~5−10 nm).[20,23,32,33] This limitation compromises the durability and performance of ultrathin and ultrasmall solid-state nanopores, which invites the

* Address correspondence to wanunu@neu.edu.

Received for review August 19, 2013 and accepted October 1, 2013.

Published online October 01, 2013
10.1021/nn404326f

exploration of biomolecular transport through other membrane materials, for example, aluminum oxide,[34] graphene,[35−37] boron nitride,[38] and, lately, DNA origami.[39−41] However, while each of these alternative materials presents unique advantages, none have the combined benefits of hydrophilicity, low-leakage, chemical resistance to strong cleaning acids, robust mechanical stability, and a simple means of fabrication.

Hafnium oxide (HfO_2) is a wide band gap high-dielectric insulator with excellent chemical resistance[42] and comparable strength to SiN_x.[42−44] While SiN_x is as strong, it is plagued by a problem of stability at the nanoscale: the oxide of silicon is chemically favored over its nitride. This tendency of nitrides to oxidize is exemplified by the standard enthalpy of formations of Si_3N_4 (−198 kcal/mol),[45] SiO_2 (−217 kcal/mol),[46] HfN (88.2 kcal/mol),[47] and HfO_2 (−266 kcal/mol).[47] Therefore, while SiN_x is normally a robust material, in an oxygen-rich environment the nitride surface is an evolving mixture of nitrogen and oxygen, the proportion of which can vary during nanopore fabrication[29] and following cleaning using oxygen-rich agents (*e.g.*, O_2 plasma and hot piranha solution). In contrast, the chemical form of HfO_2 is stable, which can improve reliability and reproducibility during nanopore experiments and, in principle, offer a well-regulated interaction of the pore walls with biomolecules. Finally, the isoelectric point of ∼7 for HfO_2[48] renders its surface near-neutral under physiological pH, which suggests compatibility of solid-state nanopores with studying transport of negatively charged biomolecules such as nucleic acids. Recently, Shim *et al.* demonstrated DNA translocations through a graphene/HfO_2 pore, demonstrating the viability of this material for nanopore devices.[49]

In this article we investigate single-stranded and double-stranded DNA transport through nanopores in ultrathin HfO_2 membranes at high temporal resolution. Figure 1a shows the scheme of our nanopore setup, as well as typical traces during experiments with (b) double-stranded and (c) single-stranded DNA. First, we present the fabrication details of ultrathin HfO_2 membranes and nanopores in such membranes. Next, we show that transport speeds of single-stranded and double-stranded DNA are slower than for SiN_x pores of equivalent geometries, and we argue that this slowing down is due to coordinative interaction of the DNA backbone phosphates with the HfO_2 surface. Finally, we show for the first time that HfO_2 pores with diameters as small as 1.4 nm are stable in size for several hours of continuous DNA translocation experiments, during which an estimated 50 000 DNA molecules are "flossed" through the pore without any detectable erosion of the pore walls. These results suggest that HfO_2 is a superior material to SiN_x for nanopore biosensors.

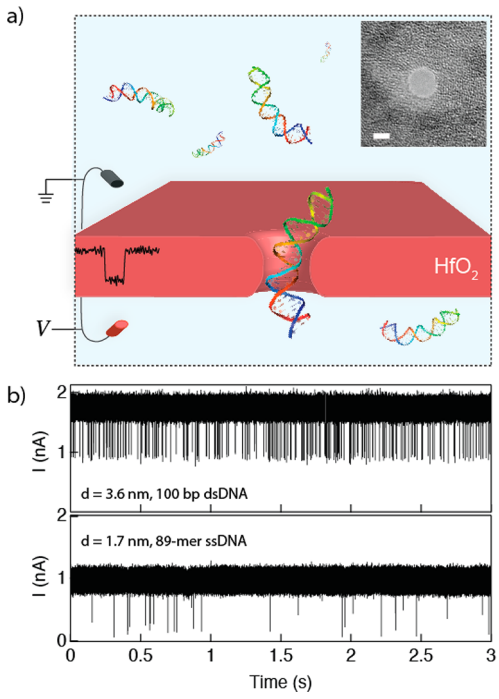

Figure 1. Hafnium oxide nanopores. (a) Cartoon schematic of the experiment. A sample of DNA is placed on the negatively charged electrode side, and ion current through the pore is monitored. Electrophoretic transport of a DNA molecule produces a single spike. Inset shows a transmission electron microscope (TEM) image of a 3.6 nm diameter HfO_2 nanopore (scale bar = 2 nm). (b) Continuous 3 s current traces of 100 bp dsDNA (top) and 89-mer ssDNA (bottom) translocating through HfO_2 pores at respective biases of $V = +175$ mV and $+150$ mV (pore diameters *d* indicated in the figure).

RESULTS AND DISCUSSION

HfO_2 Nanopore Fabrication. We present a three-step fabrication process for HfO_2 pores in Figure 2a. First, atomic-layer deposition (ALD) was used to deposit a 4.5 nm thickness of HfO_2 film onto a free-standing low-stress SiN_x window (see Supporting Information).[50] Next, electron-beam resist was spun on the membrane, and a <2 μm square portion of the SiN_x window was irradiated using e-beam lithography and subsequently developed, after which the entire thickness of the exposed SiN_x was etched using an SF_6 reactive ion etch (RIE) plasma. We have found that RIE overetching of the SiN_x layer did not remove the HfO_2 film. The membrane's elemental composition was investigated using energy dispersive X-ray spectroscopy (EDS) with a transmission electron microscope. Figure 2b shows a dark-field scanning TEM (STEM) image in which stark contrast between the thick SiN_x support and the free-standing HfO_2 membrane is visible. In addition, an atomic force microscope (AFM) scan of the same area is shown, in which the removed thickness of the SiN_x layer is confirmed. Hafnium and oxygen were present throughout the image in similar amounts, while the signals for silicon and nitrogen were virtually absent in the etched area. By combining a map of the integrated

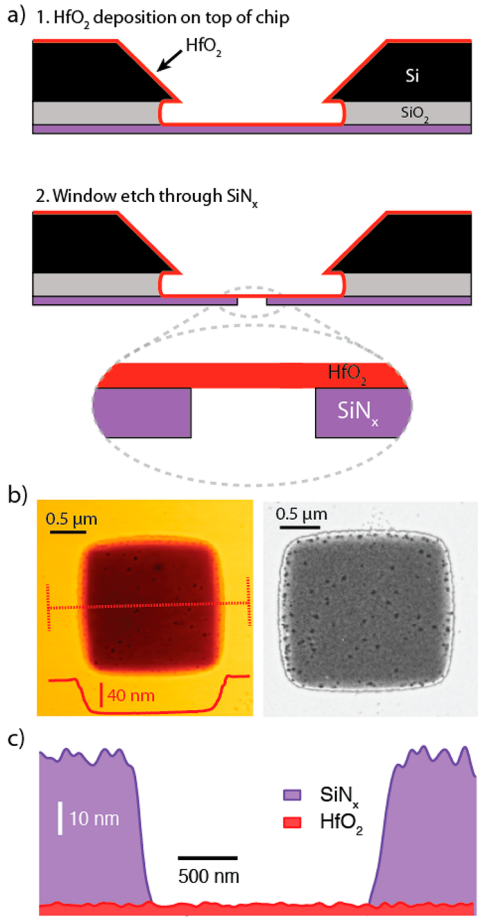

Figure 2. Freestanding HfO_2 membrane fabrication. (a) 1. Atomic layer deposition is used to deposit a 3−8 nm thick HfO_2 layer onto the trench side of a freestanding silicon nitride (SiN_x) window. 2. Reactive ion etching of a predefined window to expose the freestanding HfO_2. (b) Atomic force microscopy (AFM) topograph (left) and dark-field scanning transmission electron micrograph (right) of a freestanding HfO_2 region. Dashed red line represents line scan that confirms the 50 nm etch step height. (c) Energy dispersive spectroscopy (EDS)-based thickness map of SiN_x and HfO_2 (thickness estimated from AFM).

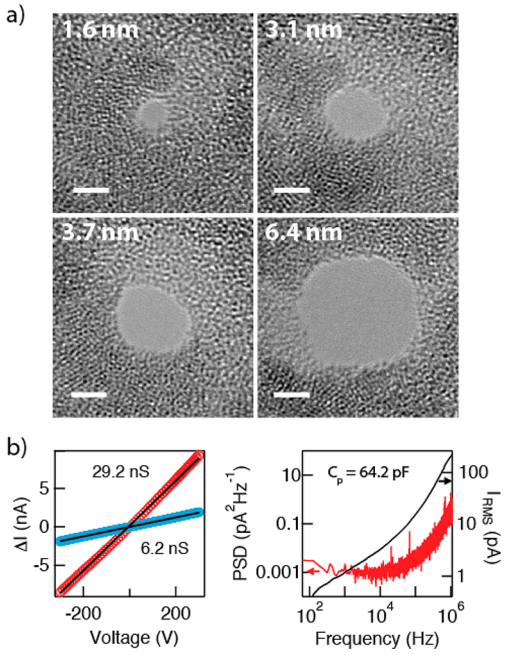

Figure 3. Pore characterization. (a) Bright-field TEM images of nanopores of diameters 1.6−6.4 nm, drilled in a HfO_2 membrane. Contrast in the membrane portion of the image is due to thickness variations, a result of e-beam-induced crystallization of the HfO_2 film. (b) Current−voltage curves of two HfO_2 pores in 1 M KCl buffer, pH 8.0 (d = 5.9 nm, d = 2.0 nm), showing linear conductance. (c) Noise power spectral density (PSD, left axis) and integrated noise (right axis) of a d = 4.0 nm pore at an applied bias of V = 250 mV (range 60−10^6 Hz). On the basis of the noise spectrum of this pore, we estimate a membrane capacitance of C_p = 64.2 pF.

EDS spectra (see Supporting Information) with AFM topography data, a reconstructed thickness map of the membrane layers is presented in Figure 2c. We note that noise of the signal in the height map arises from instrumental noise and actual roughness of the deposited SiN_x and HfO_2 films. Finally, since both the ALD and lithography steps are scalable to a whole wafer, these steps were carried out in parallel to produce a large number of HfO_2 membranes for experiments.

The third and final fabrication step was nanopore drilling using a transmission electron microscope. Hard irradiation (2.5×10^8 e/nm^2) of a ~2×2 nm^2 region of the membrane resulted in slow formation of a nanopore, the kinetics of which are ~10 times slower than for similar thickness silicon nitride membranes.[51] In contrast to SiN_x, soft electron-beam irradiation of freestanding HfO_2 using 200 kV electrons (10^6 e/nm^2) for 40−60 s leads to a phase transition from an amorphous to a polycrystalline state (see Supporting Information), as previously observed for Al_2O_3[34] and HfO_2/graphene nanopores.[49] While we were able to produce pores in these crystallized HfO_2 nanodomains, their ionic conductance was always larger than anticipated. We hypothesize that these pores are unstable as a result of mechanical failure of the crystalline domain due to strain mismatch with the amorphous membrane.

Example bright-field TEM images of nanopores in the diameter range of 1.4−6.5 nm are shown in Figure 3a. Contrasting patches in the image correspond to thickness variations in the semicrystallized HfO_2 film, which are clearly induced by extended e-beam irradiation. Following nanopore fabrication, the devices were cleaned in hot piranha and then rinsed copiously in hot deionized water, and after vacuum drying they were immediately assembled in a custom PTFE cell. Current−voltage curves were used to measure the pore conductance, as shown in Figure 3b for a 5.9 nm and a 2.0 nm pore fabricated in 4.5 nm thick HfO_2 membranes. Linearity of the current−voltage curves was consistent with a symmetric and/or weakly charged pore surface. For a given batch of HfO_2 membranes we found a good agreement between pore conductance and diameter, although the pore thickness varied by as much as 50%, as determined by sizing from DNA translocation experiments (see Supporting Information). The pores

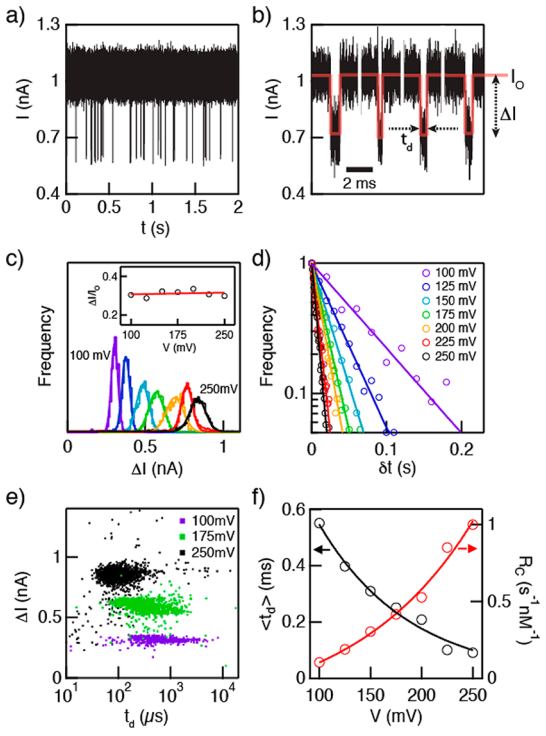

Figure 4. Transport of 150 nM 100 bp double-stranded DNA (dsDNA) through a d = 3.6 nm HfO_2 nanopore. (a) Continuous two-second current trace at V = 100 mV. (b) Representative concatenated events following analysis using OpenNanopore[53] software. Each event is defined by its mean current amplitude (ΔI) and dwell time (t_d). Red line represents square wave fit to each event. (c) Histograms of ΔI at different voltages in the range V = 100−250 mV, showing a regular increase in ΔI with increasing voltage. Inset shows the fractional blockage, $\Delta I/I_o$, which is found to be independent of voltage. (d) Distributions of event interarrival times at different voltages (δt). Lines are fits to the distributions, from which the capture rates R_c are extracted. (e) Scatter plots of ΔI *vs* t_d for selected voltages. The decrease in spread of t_d values with increasing voltages exemplifies the transition from diffusion-dominated to drift-dominated transport. (f) Peak t_d (left axis) and R_c (right axis) values as a function of voltage (see Supporting Information), showing exponential dependence for both parameters (see text).

exhibited low noise, as shown in Figure 3c by the power spectral density (PSD) and integrated current noise for a 4.0 nm diameter pore at an applied voltage of 250 mV. By painting most of the chip surface with an elastomer gasket[52] we were able to reduce the capacitance of our chips to the range 60−150 pF, which is sufficient to enable measurements at wide signal bandwidths (≥200 kHz).

Double-Stranded DNA Transport. We first characterize the voltage-driven transport of double-stranded DNA (dsDNA) through our HfO_2 pores. While a good correspondence is found between the TEM-measured pore size and the observed conductance, quoted pore sizes throughout the paper were independently assessed from the blocked current level during DNA translocation experiments.[20] In Figure 4a, a representative two-second current trace is shown of a 3.6 nm diameter pore at V = 100 mV following the addition of 150 nM of 100 bp dsDNA to the negatively biased *cis* chamber. For each experiment, >60 s of data similar to what is shown in Figure 4a was analyzed offline using OpenNanopore, an open source translocation data analysis package from the Radenovic Lab at EPFL.[53] OpenNanopore fits all detected single-level spikes from the trace with rectangular pulses, as illustrated in Figure 4b (multilevel events were rare and as such they were ignored). The duration of the pulse corresponds to the dwell time (t_d), while the amount of reduction in the baseline current from the open-pore level (I_o) is referred to as ΔI. The molecule's arrival time, δt, is the wait time between consecutive event beginnings.

Figure 4c plots histograms of ΔI for each experimental voltage. We see that ΔI increases linearly with voltage (as does I_o, not shown). However, as shown in the inset to the figure, the fractional blockade ($\langle\Delta I\rangle/I_o$) is independent of voltage in the range 100−250 mV. As mentioned above, the pore diameter can be characterized based on the fractional blockade value, assuming a dsDNA cross-sectional diameter of 2.2 nm.[20] Assuming that the current blocked is entirely due to a fractional excluded volume of DNA from the pore, we use measured I_o and ΔI values to determine the pore diameter d and its effective height h_{eff}:[20,21]

$$I_o = V\sigma\left(\frac{4h_{eff}}{\pi d^2} + \frac{1}{d}\right)^{-1};$$

$$\Delta I = V\sigma\left(\frac{4h_{eff}}{\pi(2.2\text{ nm})^2} + \frac{1}{2.2\text{ nm}}\right)^{-1}$$

where V is the applied voltage and σ = 0.096 S/cm is the measured specific conductance of the buffer at 25 °C. For the pore in the experiment shown in Figure 4, we find h_{eff} = 7 nm (the highest pore thickness we observed) and d = 3.6 nm. Further, we determine the capture rate R_c from each experiment by fitting the arrival time distributions to a first arrival time process $P(t) = A\exp(-R_c t)$, as seen in Figure 4d.[54] The inverse time constant of each fit corresponds to the event rate. In small pores, DNA capture rates are limited by an energetic penalty of DNA confinement within the pore, and the event rate is expected to depend exponentially on voltage,[54] whereas in large pores capture is limited by arrival time to the pore mouth (Smoluchowski limit), in which case capture rate is linearly dependent on voltage.[55] We indeed observe exponential capture rate dependence with voltage (plotted on the left axis of Figure 4f), as previously observed for similar-diameter pores.[19] While a quantitative comparison was not pursued here, we find that the capture rates in our HfO_2 pores are higher than or similar to those in prior studies.[19,56]

Scatter plots of ΔI *vs* t_d for selected voltages in the range 100−250 mV are displayed in Figure 4e. Upon increasing the applied voltage, a noticeable decrease

of the spread in t_d distributions is observed, coupled to an increase in ΔI spread. We attribute this reduction in the spread of t_d to a transition from diffusion-dominated transport to drift-dominated transport: at low bias values (100−150 mV), DNA transport is hindered by interactions with the pore walls and hydrodynamic interactions that present a barrier for transport, whereas at high bias values (200−250 mV) electrophoretic forces dominate DNA transport.[57] In order to obtain the most likely dwell times, we have plotted log-normal distributions (see Supporting Information) and extracted the peak positions, which are plotted in Figure 4f (left *y*-axis). As seen in the plot, the characteristic dwell times in the voltage range 100−250 mV correspond to average DNA velocities of 5.5−1 μs/bp, respectively. The minimum characteristic velocity we obtained (V = 100 mV, 181 bp/ms) compares favorably with other works, as seen in a recent compilation by Venkatesan *et al.*[2] Comparison of our measured DNA average velocity with a similar-diameter SiN_x pore shows a steeper dependence on voltage for HfO_2, which may be due to the stronger interactions of DNA with the HfO_2 pore walls (see Supporting Information). Although the exact mechanism of this interaction is not clear, prior studies of a series of M(IV) oxides such as ZrO_2, TiO_2, and HfO_2 indicate a reasonable affinity toward phosphate groups,[58−61] which may mediate DNA slowing by increasing frictional forces with the pore walls during the translocation process.

Single-Stranded DNA Transport. Nanopore detection of single-stranded DNA (ssDNA) has been studied extensively as a potential technology for DNA sequencing.[4,5,62] To show that HfO_2 nanopores are compatible with single-stranded DNA experiments, we evaluated the transport kinetics of an 89-mer single-stranded DNA molecule through two different HfO_2 pores with diameters of 1.4 and 1.7 nm. Representative one-second snapshots of the traces collected for both pores at different voltages are shown in Figure 5a. The traces show events with very deep blockages for both pores. Specifically, for the 1.4 nm pore the mean fractional blockade is 83%, while for the 1.7 nm pore the mean fractional blockade is 70%. These fractional blockades are close in magnitude to α-hemolysin (αHL), for which we have independently measured a $\langle \Delta I \rangle / I_o$ value of 80% (see Supporting Information). It is noteworthy to remark that while αHL nanopores do not exhibit efficient capture from the β-barrel (*trans*) side of the membrane without a vestibule,[63] capture of molecules into both HfO_2 pore sizes was at least as efficient as capture into the vestibule (*cis*) side of αHL. At 200 mV, we measure a rate of ~20 s^{-1} μM^{-1} for HfO_2 ~, while previous experiments have measured 7 s^{-1} μM^{-1} for αHL at 200 mV.[54]

Similarly to dsDNA, a ssDNA molecule experiences strong interactions with the HfO_2 pore walls, which causes an enormous distribution of dwell times. In Figure 5b, scatter plots of fractional current blockades *vs* dwell times are shown for the same 89-mer ssDNA sample transported through 1.7 and 1.4 nm diameter pores. It is striking that a ~0.3 nm reduction in pore diameter increases the most likely dwell times by ~30 and the spread in dwell times by ~100. This large variance in dwell time can be attributed to strong interactions between the ssDNA molecule and the walls of the HfO_2 pore, which may cause stick−slip motion of the ssDNA through the pore. In addition to phosphate backbone interactions, we cannot rule out interactions of the HfO_2 surface with specific nucleobases.[61] While not dynamically controllable as in other proposed devices,[64] this enhanced interaction of DNA with HfO_2 pores can be useful for slowing DNA motion through the pore. Upon fitting the dwell time data to log-normal distributions (see Supporting Information), the dependence of the most likely dwell time ($\langle t_d \rangle$) on voltage is shown in Figure 5d. In the figure, one-sided error bars represent the long-tail variance of the distributions.

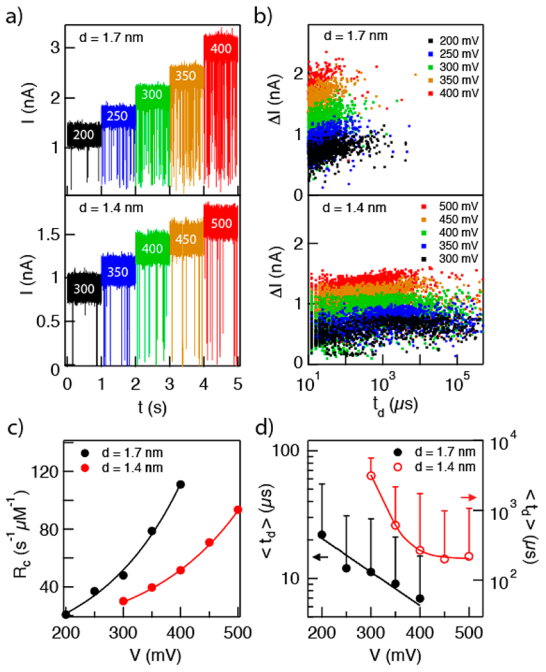

Figure 5. Transport of 89-mer single-stranded DNA (ssDNA) through HfO_2 pores with d = 1.4 and 1.7 nm. (a) Continuous current traces at various voltages (indicated in white text on traces). Deep fractional blockades are observed; $\Delta I/I_o$ = 83% for d = 1.4 nm and 70% for d = 1.7 nm pore. (b) Scatter plots of ΔI *vs* t_d demonstrate the impact of a 0.3 nm pore diameter reduction on the spread of dwell times. This strong dependence is evidence of strong interactions between the ssDNA molecule and the HfO_2 pore. (c) Normalized capture rates as a function of voltage. Both pores exhibit exponential dependence of event rate on voltage, owing to an energetic barrier for capture into the pores (error bars smaller than markers). (d) Mean dwell times for 1.7 nm pore (left axis) and 1.4 nm pore (right axis). Evidence of strong interactions is seen by the orders of magnitude longer dwell times and wider spread of the distributions (see Supporting Information), as well as the superexponential dependence of dwell times on voltage for the 1.4 nm pore.

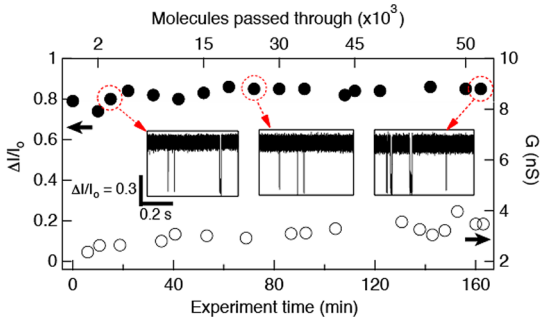

Figure 6. Time stability data for a 1.4 nm diameter HfO_2 pore. Plot shows the fractional current blockade $\Delta I/I_o$ (left axis) as a function of the ~2.5 h experiment time. The pore conductance as a function of time is shown on the right axis. Insets show current traces at different times of the experiment ($V = 350$ mV). Top axis shows the estimated number of molecules passed through the pore.

While exponential dependence is observed for the 1.7 nm diameter pore (left axis), we find superexponential behavior of $\langle t_d \rangle$ for the 1.4 nm pore (right axis). Recent Langevin dynamics simulations of a strongly interacting pore find a superexponential relationship between driving force and dwell time,[65] which produce remarkably similar behavior to our experiments. Though further investigation is required, two nonexclusive mechanisms can explain this behavior: (1) the pore we have used is too small to allow unhindered passage of ssDNA nucleobases, resulting in steric-dominated stick–slip motion through the pore,[66] and (2) chemical interactions between ssDNA and the HfO_2 surface are responsible for this observed friction.[61]

Finally, since the properties of synthetic nanopores are more susceptible to change over the course of an experiment than those of protein pores,[31] we investigated the abrasion resistance of a sub-2 nm HfO_2 pore during a multihour experiment. In Figure 6, we plot the fractional current blockade ($\Delta I/I_o$) as a function of experiment time for a 1.4 nm diameter pore at $V = 350$ mV (closed circles, left axis). The pore conductance ΔG over time is also plotted (open circles, right axis). During this experiment, >50 000 ssDNA molecules have been passed through the pore, and yet the unchanged $\Delta I/I_o$ indicates that the pore diameter remains constant; the minor <10% conductance change is merely the result of water evaporation from the buffer. Given the strong interactions of ssDNA with the 1.4 nm pore, one would expect the pore to clog easily. Counterintuitively, these pores simultaneously demonstrate strong pore–analyte interactions and resistance to clogging. We attribute this to the pore thinness, which serves to both confine the region of strongest interaction and increase the electric field (*i.e.*, driving force) within the pore. This result exemplifies the strong chemical and mechanical stability of the HfO_2 membrane.

CONCLUSIONS

In conclusion, we have demonstrated that HfO_2 is a viable alternative to SiN_x for solid-state nanopore sensors. Fabrication of a wafer-full of HfO_2 membranes and nanopore fabrication in these membranes using a TEM are straightforward. HfO_2 pores are hydrophilic, stable, and have nearly neutral surface charge in physiological conditions. By studying voltage-driven transport of DNA molecules, we have shown that 3.6 nm diameter HfO_2 pores efficiently admit dsDNA molecules at lower bias voltages than SiN_x pores, while transport is slower than for SiN_x pores of similar geometry. Likewise, with 1.4 nm diameter pores we have measured much longer and more spread out ssDNA transport time statistics than with a 1.7 nm diameter pore, suggesting very strong interactions between the material and the nucleic acid molecules. The combined experiments point to interaction between the DNA backbone and HfO_2, which we posit comes from phosphate/HfO_2 interactions. Finally, the pores exhibit a remarkable stability over time, which enables the fabrication of small pores in thin membranes that are usable for hours of continuous measurements. Further studies of the interactions between DNA and HfO_2 in the context of voltage-driven or enzyme-driven DNA translocation[67] may improve the detection of DNA polymers through solid-state nanopores,[23] enable a more controlled transport through nanopores equipped with transverse electrodes,[68–70] enable high-resolution studies of DNA/protein interactions *via* rupturing forces,[66,71] and be used in conjunction with small graphene pores for a further reduction of DNA velocity,[22,72] as well as for other nanopore-based applications.

MATERIALS AND METHODS

Substrates for nanopore fabrication were 5 × 5 mm^2 Si chips with a 50 nm thick SiN_x film deposited on a 2.5 μm thick thermal SiO_2 layer, which helps to reduce electrical noise. HfO_2 films were deposited at 150 °C using a GEMSTAR benchtop ALD system (Arradiance), with tetrakis(ethylmethylamino)hafnium and H_2O used as a precursor and oxidizer, respectively.[50] AFM- and ellipsometry-calibrated thicknesses of SiN_x were etched in a Technics Micro-RIE Series 800 etcher using sulfur hexafluoride (SF_6) at 300 mTorr and 150 W. SiN_x was protected with a 950 PMMA etch mask, and a small region was exposed using Nabity NPGS e-beam writing software on a Hitachi S-4800 scanning electron microscope. Exposed PMMA was developed with 3:1 isopropyl alcohol and methyl isobutylketone, and following SiN_x thinning PMMA was removed using acetone.[20] Nanopores were fabricated and imaged at Northeastern University using a JEOL 2010FEG transmission electron microscope at 200 kV.

Nanopore chips were cleaned using hot piranha followed by hot water. After vacuum drying, the chips were mounted in a PTFE cell using a quick-curing elastomer gasket (Smooth-On EcoFlex 5). Cell chambers were filled with 1 M KCl buffer solution (pH 8.3, 10 mM Tris, 1 mM EDTA), and Ag/AgCl electrodes were

inserted into each chamber. Current data were collected at 4 MS/s and digitally low-pass filtered using a Chimera Instruments VC100 amplifier system[23] unless otherwise indicated. Before addition of a DNA sample, a current−voltage curve and a several second current trace at constant bias were collected to ensure a steady open pore current. Sample molecules were then thoroughly mixed with the buffer in the chamber using a pipet to achieve a final desired concentration. Molecules and concentrations were as follows: for ssDNA experiments, a 30−100 nM 89-mer solution was used (see Supporting Information). For dsDNA experiments, a 150 nM solution of 100 bp Fermentas NoLimits DNA fragment was used (Thermo Scientific).

Conflict of Interest: The authors declare the following competing financial interest(s): J.K.R. is a principal in Chimera Instruments.

Supporting Information Available: Membrane characterization details, raw traces, analysis details, and comparison with other pores. This material is available free of charge *via* the Internet at http://pubs.acs.org.

Acknowledgment. The authors acknowledge financial support from The National Human Genome Research Institute grant number R21 HG006873. The authors thank Cohavit Gil and Baram Sosis for help in atomic layer deposition calibration, Andrey Ivankin for α-hemolysin translocation data, and Carolyn Shasha for adaptation of the OpenNanopore source code to our data. The authors acknowledge the Center for Nanoscale Systems (CNS) at Harvard University, a part of the National Nanotechnology Infrastructure Network, where EDS data were acquired. The authors thank Murugappan Muthukumar for fruitful discussions.

REFERENCES AND NOTES

1. Howorka, S.; Siwy, Z. Nanopore Analytics: Sensing of Single Molecules. *Chem. Soc. Rev.* **2009**, *38*, 2360–2384.
2. Venkatesan, B. M.; Bashir, R. Nanopore Sensors for Nucleic Acid Analysis. *Nat. Nanotechnol.* **2011**, *6*, 615–624.
3. Haque, F.; Li, J. H.; Wu, H. C.; Liang, X. J.; Guo, P. X. Solid-State and Biological Nanopore for Real-Time Sensing of Single Chemical and Sequencing of DNA. *Nano Today* **2013**, *8*, 56–74.
4. Kasianowicz, J. J.; Brandin, E.; Branton, D.; Deamer, D. W. Characterization of Individual Polynucleotide Molecules Using a Membrane Channel. *Proc. Natl. Acad. Sci. U.S.A.* **1996**, *93*, 13770–13773.
5. Branton, D.; Deamer, D. W.; Marziali, A.; Bayley, H.; Benner, S. A.; Butler, T.; Di Ventra, M.; Garaj, S.; Hibbs, A.; Huang, X. H.; *et al*. The Potential and Challenges of Nanopore Sequencing. *Nat. Biotechnol.* **2008**, *26*, 1146–1153.
6. Zwolak, M.; Di Ventra, M. Colloquium: Physical Approaches to DNA Sequencing and Detection. *Rev. Mod. Phys.* **2008**, *80*, 141–165.
7. Schneider, G. F.; Dekker, C. DNA Sequencing with Nanopores. *Nat. Biotechnol.* **2012**, *30*, 326–328.
8. Singer, A.; Rapireddy, S.; Ly, D. H.; Meller, A. Electronic Barcoding of a Viral Gene at the Single-Molecule Level. *Nano Lett.* **2012**, *12*, 1722–1728.
9. Kowalczyk, S. W.; Hall, A. R.; Dekker, C. Detection of Local Protein Structures along DNA Using Solid-State Nanopores. *Nano Lett.* **2010**, *10*, 324–328.
10. Bates, M.; Burns, M.; Meller, A. Dynamics of DNA Molecules in a Membrane Channel Probed by Active Control Techniques. *Biophys. J.* **2003**, *84*, 2366–2372.
11. Tropini, C.; Marziali, A. Multi-Nanopore Force Spectroscopy for DNA Analysis. *Biophys. J.* **2007**, *92*, 1632–1637.
12. Dudko, O. K.; Mathe, J.; Szabo, A.; Meller, A.; Hummer, G. Extracting Kinetics from Single-Molecule Force Spectroscopy: Nanopore Unzipping of DNA Hairpins. *Biophys. J.* **2007**, *92*, 4188–4195.
13. Tabard-Cossa, V.; Wiggin, M.; Trivedi, D.; Jetha, N. N.; Dwyer, J. R.; Marziali, A. Single-Molecule Bonds Characterized by Solid-State Nanopore Force Spectroscopy. *ACS Nano* **2009**, *3*, 3009–3014.
14. Soni, G. V.; Dekker, C. Detection of Nucleosomal Substructures Using Solid-State Nanopores. *Nano Lett.* **2012**, *12*, 3180–3186.
15. Storm, A. J.; Chen, J. H.; Ling, X. S.; Zandbergen, H. W.; Dekker, C. Fabrication of Solid-State Nanopores with Single-Nanometre Precision. *Nat. Mater.* **2003**, *2*, 537–540.
16. Li, J.; Stein, D.; McMullan, C.; Branton, D.; Aziz, M. J.; Golovchenko, J. A. Ion-Beam Sculpting at Nanometre Length Scales. *Nature* **2001**, *412*, 166–169.
17. Yang, J. J.; Ferranti, D. C.; Stern, L. A.; Sanford, C. A.; Huang, J.; Ren, Z.; Qin, L. C.; Hall, A. R. Rapid and Precise Scanning Helium Ion Microscope Milling of Solid-State Nanopores for Biomolecule Detection. *Nanotechnology* **2011**, *22*, 285310.
18. Aksimentiev, A.; Heng, J. B.; Cruz-Chu, E. R.; Timp, G.; Schulten, K. Microscopic Kinetics of DNA Translocation through Synthetic Nanopores. *Biophys. J.* **2005**, *88*, 352a–352a.
19. Wanunu, M.; Sutin, J.; McNally, B.; Chow, A.; Meller, A. DNA Translocation Governed by Interactions with Solid-State Nanopores. *Biophys. J.* **2008**, *95*, 4716–4725.
20. Wanunu, M.; Dadosh, T.; Ray, V.; Jin, J. M.; McReynolds, L.; Drndic, M. Rapid Electronic Detection of Probe-Specific Micrornas Using Thin Nanopore Sensors. *Nat. Nanotechnol.* **2010**, *5*, 807–814.
21. Kowalczyk, S. W.; Grosberg, A. Y.; Rabin, Y.; Dekker, C. Modeling the Conductance and DNA Blockade of Solid-State Nanopores. *Nanotechnology* **2011**, *22*, 315101.
22. Garaj, S.; Liu, S.; Golovchenko, J. A.; Branton, D. Molecule-Hugging Graphene Nanopores. *Proc. Natl. Acad. Sci. U.S.A.* **2013**, *110*, 12192–12196.
23. Venta, K.; Shemer, G.; Puster, M.; Rodriguez-Manzo, J. A.; Balan, A.; Rosenstein, J. K.; Shepard, K.; Drndic, M. Differentiation of Short, Single-Stranded DNA Homopolymers in Solid-State Nanopores. *ACS Nano* **2013**, *7*, 4629–4636.
24. Kim, Y. R.; Min, J.; Lee, I. H.; Kim, S.; Kim, A. G.; Kim, K.; Namkoong, K.; Ko, C. Nanopore Sensor for Fast Label-Free Detection of Short Double-Stranded DNAs. *Biosens. Bioelectron.* **2007**, *22*, 2926–2931.
25. Wei, R. S.; Gatterdam, V.; Wieneke, R.; Tampe, R.; Rant, U. Stochastic Sensing of Proteins with Receptor-Modified Solid-State Nanopores. *Nat Nanotechnol.* **2012**, *7*, 257–263.
26. Anderson, B. N.; Muthukumar, M.; Meller, A. pH Tuning of DNA Translocation Time through Organically Functionalized Nanopores. *ACS Nano* **2013**, *7*, 1408–1414.
27. Rosenstein, J. K.; Wanunu, M.; Merchant, C. A.; Drndic, M.; Shepard, K. L. Integrated Nanopore Sensing Platform with Sub-Microsecond Temporal Resolution. *Nat. Methods* **2012**, *9*, 487–492.
28. Storm, A. J.; Storm, C.; Chen, J. H.; Zandbergen, H.; Joanny, J. F.; Dekker, C. Fast DNA Translocation through a Solid-State Nanopore. *Nano Lett.* **2005**, *5*, 1193–1197.
29. Wu, M. Y.; Krapf, D.; Zandbergen, M.; Zandbergen, H.; Batson, P. E. Formation of Nanopores in a SiN/SiO_2 Membrane with an Electron Beam. *Appl. Phys. Lett.* **2005**, *87*, 113106.
30. Liebes, Y.; Hadad, B.; Ashkenasy, N. Effects of Electrons on the Shape of Nanopores Prepared by Focused Electron Beam Induced Etching. *Nanotechnology* **2011**, *22*, 285303.
31. van den Hout, M.; Hall, A. R.; Wu, M. Y.; Zandbergen, H. W.; Dekker, C.; Dekker, N. H. Controlling Nanopore Size, Shape and Stability. *Nanotechnology* **2010**, *21*, 115304.
32. Kuan, A. T.; Golovchenko, J. A. Nanometer-Thin Solid-State Nanopores by Cold Ion Beam Sculpting. *Appl. Phys. Lett.* **2012**, *100*, 1–4.
33. Niedzwiecki, D. J.; Iyer, R.; Borer, P. N.; Movileanu, L. Sampling a Biomarker of the Human Immunodeficiency Virus across a Synthetic Nanopore. *ACS Nano* **2013**, *7*, 3731–3731.
34. Venkatesan, B. M.; Dorvel, B.; Yemenicioglu, S.; Watkins, N.; Petrov, I.; Bashir, R. Highly Sensitive, Mechanically Stable Nanopore Sensors for DNA Analysis. *Adv. Mater.* **2009**, *21*, 2771–2776.

35. Garaj, S.; Hubbard, W.; Reina, A.; Kong, J.; Branton, D.; Golovchenko, J. A. Graphene as a Subnanometre Trans-Electrode Membrane. *Nature* **2010**, *467*, 190–193.
36. Merchant, C. A.; Healy, K.; Wanunu, M.; Ray, V.; Peterman, N.; Bartel, J.; Fischbein, M. D.; Venta, K.; Luo, Z. T.; Johnson, A. T. C.; *et al*. DNA Translocation through Graphene Nanopores. *Nano Lett.* **2010**, *10*, 2915–2921.
37. Schneider, G. F.; Kowalczyk, S. W.; Calado, V. E.; Pandraud, G.; Zandbergen, H. W.; Vandersypen, L. M. K.; Dekker, C. DNA Translocation through Graphene Nanopores. *Nano Lett.* **2010**, *10*, 3163–3167.
38. Liu, S.; Lu, B.; Zhao, Q.; Li, J.; Gao, T.; Chen, Y.; Zhang, Y.; Liu, Z.; Fan, Z.; Yang, F.; *et al*. Boron Nitride Nanopores: Highly Sensitive DNA Single-Molecule Detectors. *Adv. Mater.* **2013**, 10.1002/adma.201301336.
39. Wei, R. S.; Martin, T. G.; Rant, U.; Dietz, H. DNA Origami Gatekeepers for Solid-State Nanopores. *Angew. Chem., Int. Ed.* **2012**, *51*, 4864–4867.
40. Langecker, M.; Arnaut, V.; Martin, T. G.; List, J.; Renner, S.; Mayer, M.; Dietz, H.; Simmel, F. C. Synthetic Lipid Membrane Channels Formed by Designed DNA Nanostructures. *Science* **2012**, *338*, 932–936.
41. Bell, N. A. W.; Engst, C. R.; Ablay, M.; Divitini, G.; Ducati, C.; Liedl, T.; Keyser, U. F. DNA Origami Nanopores. *Nano Lett.* **2012**, *12*, 512–517.
42. Nielsen, R. H.; Wilfing, G. Hafnium and Hafnium Compounds. In *Ullmann's Encyclopedia of Industrial Chemistry*; Wiley-VCH Verlag GmbH & Co. KGaA, 2000.
43. Chuang, W. H.; Luger, T.; Fettig, R. K.; Ghodssi, R. Mechanical Property Characterization of LPCVD Silicon Nitride Thin Films at Cryogenic Temperatures. *J. Microelectromech. S* **2004**, *13*, 870–879.
44. Tapily, K.; Jakes, J. E.; Stone, D. S.; Shrestha, P.; Gu, D.; Baumgart, H.; Elmustafa, A. A. Nanoindentation Investigation of HfO2 and Al2O3 Films Grown by Atomic Layer Deposition. *J. Electrochem. Soc.* **2008**, *155*, H545–H551.
45. O'Hare, P. A. G.; Tomaszkiewicz, I.; Beck, I. C. M.; Seifert, H. J. Thermodynamics of Silicon Nitride. I. Standard Molar Enthalpies of Formation Δfhmo at the Temperature 298.15 K of A-Si3N4 and B-Si3N4. *J. Chem. Thermodyn.* **1999**, *31*, 303–322.
46. Zumdahl, S. S. *Chemical Principles*, 6th ed.; Houghton Mifflin Company, 2009; p A22.
47. Humphrey, G. L. Heats of Formation of Hafnium Oxide and Hafnium Nitride. *J. Am. Chem. Soc.* **1953**, *75*, 2806–2807.
48. Kosmulski, M. Attempt to Determine Pristine Points of Zero Charge of Nb_2O_5, Ta_2O_5, and HfO_2. *Langmuir* **1997**, *13*, 6315–6320.
49. Shim, J.; Rivera, J. A.; Bashir, R. Electron Beam Induced Local Crystallization of HfO_2 Nanopores for Biosensing Applications. *Nanoscale* **2013**, 10.1039/C3NR02608F.
50. Hausmann, D. M.; Kim, E.; Becker, J.; Gordon, R. G. Atomic Layer Deposition of Hafnium and Zirconium Oxides Using Metal Amide Precursors. *Chem. Mater.* **2002**, *14*, 4350–4358.
51. Kim, M. J.; Wanunu, M.; Bell, D. C.; Meller, A. Rapid Fabrication of Uniformly Sized Nanopores and Nanopore Arrays for Parallel DNA Analysis. *Adv. Mater.* **2006**, *18*, 3149–3155.
52. Tabard-Cossa, V.; Trivedi, D.; Wiggin, M.; Jetha, N. N.; Marziali, A. Noise Analysis and Reduction in Solid-State Nanopores. *Nanotechnology* **2007**, *18*, 305505.
53. Raillon, C.; Granjon, P.; Graf, M.; Steinbock, L. J.; Radenovic, A. Fast and Automatic Processing of Multi-Level Events in Nanopore Translocation Experiments. *Nanoscale* **2012**, *4*, 4916–4924.
54. Meller, A.; Branton, D. Single Molecule Measurements of DNA Transport through a Nanopore. *Electrophoresis* **2002**, *23*, 2583–2591.
55. Chen, P.; Gu, J. J.; Brandin, E.; Kim, Y. R.; Wang, Q.; Branton, D. Probing Single DNA Molecule Transport Using Fabricated Nanopores. *Nano Lett.* **2004**, *4*, 2293–2298.
56. Wanunu, M.; Morrison, W.; Rabin, Y.; Grosberg, A. Y.; Meller, A. Electrostatic Focusing of Unlabelled DNA into Nanoscale Pores Using a Salt Gradient. *Nat. Nanotechnol.* **2010**, *5*, 160–165.
57. Lubensky, D. K.; Nelson, D. R. Driven Polymer Translocation through a Narrow Pore. *Biophys. J.* **1999**, *77*, 1824–1838.
58. Sun, L. F.; Carr, P. W. Mixed-Mode Retention of Peptides on Phosphate-Modified Polybutadiene-Coated Zirconia. *Anal. Chem.* **1995**, *67*, 2517–2523.
59. Hofer, R.; Textor, M.; Spencer, N. D. Alkyl Phosphate Monolayers, Self-Assembled from Aqueous Solution onto Metal Oxide Surfaces. *Langmuir* **2001**, *17*, 4014–4020.
60. Yildirim, O.; Yilmaz, M. D.; Reinhoudt, D. N.; Blank, D. H. A.; Rijnders, G.; Huskens, J. Electrochemical Stability of Self-Assembled Alkylphosphate Monolayers on Conducting Metal Oxides. *Langmuir* **2011**, *27*, 9890–9894.
61. Fahrenkopf, N. M.; Rice, P. Z.; Bergkvist, M.; Deskins, N. A.; Cady, N. C. Immobilization Mechanisms of Deoxyribonucleic Acid (DNA) to Hafnium Dioxide (HfO_2) Surfaces for Biosensing Applications. *ACS Appl. Mater. Interfaces* **2012**, *4*, 5360–5368.
62. Wanunu, M. Nanopores: A Journey Towards DNA Sequencing. *Phys. Life Rev.* **2012**, *9*, 125–158.
63. Henrickson, S. E.; Misakian, M.; Robertson, B.; Kasianowicz, J. J. Driven DNA Transport into an Asymmetric Nanometer-Scale Pore. *Phys. Rev. Lett.* **2000**, *85*, 3057–3060.
64. Luan, B. Q.; Martyna, G.; Stolovitzky, G. Characterizing and Controlling the Motion of ssDNA in a Solid-State Nanopore. *Biophys. J.* **2011**, *101*, 2214–2222.
65. Luo, K. F.; Ala-Nissila, T.; Ying, S. C.; Bhattacharya, A. Translocation Dynamics with Attractive Nanopore-Polymer Interactions. *Phys. Rev. E* **2008**, *78*, 061918.
66. Mirsaidov, U.; Comer, J.; Dimitrov, V.; Aksimentiev, A.; Timp, G. Slowing the Translocation of Double-Stranded DNA Using a Nanopore Smaller Than the Double Helix. *Nanotechnology* **2010**, *21*, 395501.
67. Cherf, G. M.; Lieberman, K. R.; Rashid, H.; Lam, C. E.; Karplus, K.; Akeson, M. Automated Forward and Reverse Ratcheting of DNA in a Nanopore at 5-Angstrom Precision. *Nat. Biotechnol.* **2012**, *30*, 344–348.
68. Ivanov, A. P.; Instuli, E.; McGilvery, C. M.; Baldwin, G.; McComb, D. W.; Albrecht, T.; Edel, J. B. DNA Tunneling Detector Embedded in a Nanopore. *Nano Lett.* **2011**, *11*, 279–285.
69. Tsutsui, M.; Matsubara, K.; Ohshiro, T.; Furuhashi, M.; Taniguchi, M.; Kawai, T. Electrical Detection of Single Methylcytosines in a DNA Oligomer. *J. Am. Chem. Soc.* **2011**, *133*, 9124–9128.
70. Menard, L. D.; Mair, C. E.; Woodson, M. E.; Alarie, J. P.; Ramsey, J. M. A Device for Performing Lateral Conductance Measurements on Individual Double-Stranded DNA Molecules. *ACS Nano* **2012**, *6*, 9087–9094.
71. Shim, J.; Humphreys, G. I.; Venkatesan, B. M.; Munz, J. M.; Zou, X. Q.; Sathe, C.; Schulten, K.; Kosari, F.; Nardulli, A. M.; Vasmatzis, G.; *et al*. Detection and Quantification of Methylation in DNA Using Solid-State Nanopores. *Sci. Rep.* **2013**, *3*, 1389.
72. Venkatesan, B. M.; Estrada, D.; Banerjee, S.; Jin, X. Z.; Dorgan, V. E.; Bae, M. H.; Aluru, N. R.; Pop, E.; Bashir, R. Stacked Graphene-Al_2O_3 Nanopore Sensors for Sensitive Detection of DNA and DNA-Protein Complexes. *ACS Nano* **2012**, *6*, 441–450.